Journal of Applied Polymer Science

# Optimal design of an imprinted preassembled system by quantum chemical calculations and preparation of a surface-imprinted material for the selective removal of quinoline

**Wenming Yang,[1] Pengfei Ma,[1] Ting Fan,[2] Zhiping Zhou,[1] Hong Liu,[3] Wanzhen Xu[2]**

[1]School of Materials Science and Engineering, Jiangsu University, Zhenjiang 212013, China

[2]School of Environment and Safety Engineering, Jiangsu University, Zhenjiang 212013, China

[3]Institute of Theoretical Chemistry, State Key Laboratory of Theoretical and Computational Chemistry, Jilin University, Changchun 130023, China

Correspondence to: Z. Zhou (E-mail: zhouzp@ujs.edu.cn)

**ABSTRACT:** In this study, we examined the rational preparation of molecularly imprinted polymers (MIPs) for the selective removal of quinoline from octane. Before the preparation, density functional theory, as one of the methods of quantum chemical calculation, was used for the simulation of a quinoline-imprinted preassembly system. Methacrylic acid turned out to be the more suitable monomer for quinoline compared with acrylamide, and different template–monomer ratios, including 1:1, 1:2, and 1:3, were studied and are discussed. On the basis of the result of molecular simulation, quinoline-imprinted polymers were prepared with a combination of surface imprinting and living polymerization. The prepared quinoline–MIPs were characterized and used as selective adsorbents for batch-mode binding experiments. The fitting result of the adsorption data indicates that the adsorption kinetics and adsorption isotherms of the quinoline-imprinted polymers fit well a pseudo-second-order kinetics model and the Freundlich model, respectively. A selective recognition ability was demonstrated by equilibrium binding analysis. This study will provide needful guidance and a theoretical basis for the preparation of imprinted materials in the field of industrial denitrification. © 2014 Wiley Periodicals, Inc. J. Appl. Polym. Sci. **2015**, *132*, 41730.

**KEYWORDS:** adsorption; applications; composites

Received 5 August 2014; accepted 1 November 2014

**DOI: 10.1002/app.41730**

## INTRODUCTION

Generally, the nitrogen content (mass fraction) in oil fluctuates within 0.02–0.8%, and crude oil can occupy a value as high as 0.05–0.5%.[1] Nitrogenous compounds can have a significant effect on the stability of fuel oil, and the catalyst can be poisoned even with trace nitrogen. In addition, serious atmospheric pollution can be caused by nitric oxides generated from the burning of nitrogen-containing fuels.[2] Studies, in the meantime, have shown that nitrogen in diesel can inhibit the depth of hydrodesulfurization. However, if more than 90% nitrides in diesel are removed, the sulfur content can be lowered to less than 30 or 15 $\mu$g/g under conventional hydrogenation conditions.[3] Nitrides in oil can be primarily divided into two categories, namely, basic nitrides and nonalkali nitrides. The former includes pyridine, quinoline, aniline, acridine, and their derivatives, and the latter mainly covers pyrrole, indole, carbazole, and their derivatives. At present, hydrodenitrification,[4] oxidative denitrification,[5] biological denitrification,[6] and combination denitrification[7] are known as conventional techniques for the removal of nitrogen in petroleum products. However, current denitrification technologies all suffer different drawbacks, including a large equipment investment, tough operating conditions, and heavy environmental pollution. In addition to these disadvantages, adsorptive denitrification has a low efficiency because of a lack of selectivity.[8,9]

Because of their predetermined selectivity, favorable affinity, and high stability, molecularly imprinted polymers (MIPs) have been widely studied to offer a cost-effective, practical, and environmental friendly method of separating pollutants for environmental analysis and purification.[10–12] This powerful technique has been used to prepare different MIPs for use toward different pollutants, such as heavy-metal ions,[13] environmental estrogens,[14] and antibiotics.[15] In addition to the preparation of various kinds of MIPs for use toward different templates, novel preparation methods [e.g., surface molecular imprinting technique (SMIT) and living radical polymerization] and the design of MIPs for improving their properties have always been research hotspots in

Additional Supporting Information may be found in the online version of this article.

recent years. Through the introduction of imprinted sites to the surface of different matrix materials, SMIT successfully overcomes the disadvantages of traditional MIT, including its poor site accessibility, unfavorable adsorption kinetics, and low adsorption efficiency. Matrix materials play an important role in SMIT, and the reported matrix materials include silicon materials,[16] titanium materials,[17] carbon materials,[18] biological carrier materials,[19] and magnetic materials.[20] Potassium hexatitanate, as one of the excellent matrix materials, possesses a favorable chemical and mechanical stability, large surface area, and excellent surface activity.[21] Because of its versatility in the polymerization of polymers with controllable molecular weights, structures, and terminal groups; narrow molecular weight distribution; low requirement for the polymerization conditions; and extensive applicability for various kinds of polymerization methods and monomers, atom transfer radical polymerization (ATRP) has drawn widespread attention all over the world since 1995.[22] MIPs prepared with ATRP can obtain homogeneous network structures and imprinted site distributions; this facilitates the affinity and selectivity of MIPs.[23]

Although remarkable progress has been made in the field of molecular imprinting, the achieved progress has mainly focused on the novel design, various preparation methods, and different practical applications of MIPs, and theoretical studies on the processing of molecular imprinting and molecular recognition have been relatively few. Sufficient theoretical studies are of great significance; they can not only establish the theoretical basis of molecular imprinting itself but also provide necessary theoretical guidance for the design and preparation of MIPs. Rapidly developing computer technology and continuously improved software undoubtedly provide favorable and powerful conditions for understanding the imprinting process, identifying the type and magnitude of interactions, and selecting the optimum functional monomer and its ratio with the template.[24] The molecular simulation applied to molecular imprinting mainly involves quantum chemical calculations and molecular dynamics.[25–27] When electronic exchange is taken into account, density functional theory (DFT), as one of the methods of quantum chemical calculation, has a higher computational accuracy compared with the traditional Hartree–Fock method and possesses a faster computation speed compared with second-order Møller–Plesset theory.

In this study, DFT was used to simulate the imprinted preassembly system of the selected template, quinoline. Methacrylic acid (MAA) and acrylamide (AM) were used as functional monomers for simulation, and the simulation ratios of the template to the monomer ranged from 1:1 to 1:3. On the basis of the result of computer simulation, quinoline–MIPs were prepared with the combination of SMIT and ATRP (cf. Figure 1). Then, advanced characterization methods were used to determine the morphology and structure of the prepared materials. Batch-mode adsorption experiments were conducted, and the data were fitted and analyzed with different adsorption models. In consideration of the lack of reports on this subject, this study was supposed to provide a ponderable theoretical foundation for understanding the imprinted mechanism of quinoline and a novel, cost-effective, practical, and environmental friendly denitrification technology in the industry.

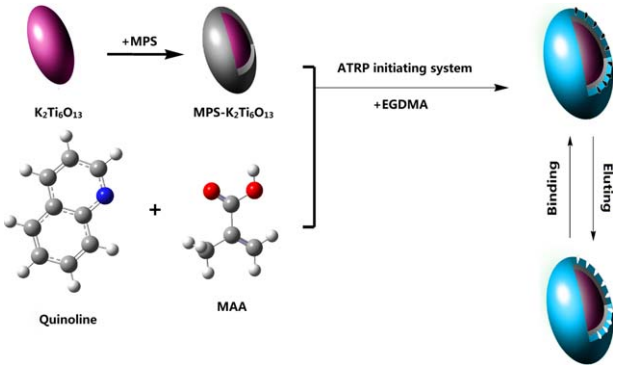


**Figure 1.** Schematic illustration of the preparation process of the quinoline–MIPs with the combination of ATRP and SMIT. [Color figure can be viewed in the online issue, which is available at wileyonlinelibrary.com.]

## EXPERIMENTAL

### Materials and Instruments

Quinoline (98%), indole (99%), benzothiophene (BT, 97%), dibenzothiophene (DBT, 99%), ethylene glycol dimethacrylate (EGDMA), CuBr, MAA, ethyl-2-bromo-2-methylpropionate, ethyl 2-bromoisobutyrate (EBiB), and 3-methacryloxypropyl trimethoxysilane (MPS) were purchased by Aladdin Reagent Co., Ltd. (Shanghai, China). AM, toluene, methanol, ethanol, glacial acetic acid (HAc), azodiisobutyronitrile, and *n*-octane were supplied from Sinopharm Chemical Reagent Co., Ltd. (Shanghai, China). $K_2Ti_6O_{13}$ was procured by Shanghai Whisker Composite Material (Shanghai, China). *N*,*N*,*N*′,*N*′,*N*″-penta-methyldiethylenetriamine (PMDETA) was obtained from Sigma-Aldrich Chemical Co. (St. Louis, MO). All of the reagents were at least analytical and were used without further treatment, with the exception of CuBr. Before use, CuBr was stirred in HAc and preserved in a vacuum-drying oven.

Field emission scanning electron microscopy (SEM) was used to observe the morphology of the MIPs with an instrument purchased from Hitachi (S-4800 Japan). Nexus 470 Fourier transform infrared (FTIR) spectrometer used to record FTIR spectra (4000–500 $cm^{-1}$) was obtained from Nicolet. A 7890A gas chromatograph containing a flame-ionization detector used to determine the concentration of quinoline was supplied by Agilent. A server with an Intel Xeon E5-2620 CPU of 2.10 GHz, 16 GB of memory, a 64-bit Windows operating system, and Gaussian09 software (Gaussian, Inc.) was used to conduct the simulation.

### Computer Simulation of the Quinoline-Imprinted Preassembly System

Gaussian 09 software was used to optimize the conformation and calculate the energy and frequency of the template–monomer complexes (the job type was set as Opt + Freq). The calculation method was restricted B3LYP of DFT at ground state with the basis set of 6-311G. The molecular simulation was conducted *in vacuo*. In addition, to further analyze and understand the imprinted mechanism, natural bond orbital (NBO) theory was used to calculate the condition of charge distribution of the complexes.

First, quinoline and two common monomers (MAA and AM) that easily formed hydrogen-bond interactions were optimized to obtain their conformations of minimum energy. After the

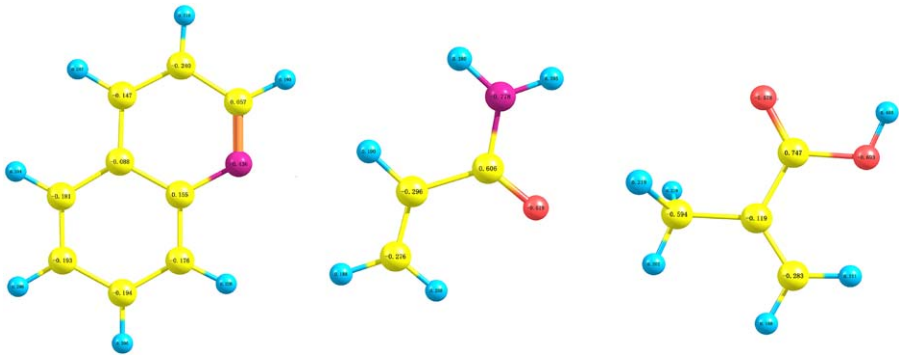

**Figure 2.** Minimum energy conformation and NBO charge distribution of quinoline, AM, and MAA. [Color figure can be viewed in the online issue, which is available at wileyonlinelibrary.com.]

completion of the calculation and convergence, the information, including the energy, frequency, and NBO charges, were obtained. The convergence criterion involved four aspects: a maximum force of less than 0.00045, a root mean square of maximum force of less than 0.0003, a maximum displacement of less than 0.0018, and a root mean square of maximum displacement of less than 0.0012. Second, on the basis of the last step, the complexes of quinoline and AM (or MAA) with different ratios ranging from 1:1 to 1:3 were further optimized. Simultaneously, counterpoise correction was used to eliminate the basis set superposition error (BSSE),[28] and the NBO charge distribution of the complexes was obtained. Finally, the imprinted preassembly systems of quinoline were analyzed with a combination of interaction energy ($\Delta E$) after BSSE correction and NBO charge distribution. For every template–monomer complex, the corresponding $\Delta E$ was obtained through the calculation of the difference value between the uncorrected energy of the quinoline–monomer complex and the energy sum of the original template and monomer(s), followed by the addition of the BSSE corrected energy. The corresponding formula is as follows:

$$\Delta E = E_{\text{complex}} - E_{\text{quinoline}} - nE_{\text{monomer}} + E_{\text{BSSE}} \quad (1)$$

where $E_{\text{complex}}$, $E_{\text{quinoline}}$, and $E_{\text{monomer}}$ are the uncorrected energy of quinoline–monomer complex and the energies of the template and monomer (kJ/mol), respectively. The value of $n$ represents the ratio between quinoline and the monomer.

### Surface Vinyl Modification of $K_2Ti_6O_{13}$

Before vinyl modification, the purchased $K_2Ti_6O_{13}$ whiskers were activated to obtain plenty of hydroxyls on their surface. Appropriate $K_2Ti_6O_{13}$ whiskers were immersed in 3 mol/L HCl, and the activated $K_2Ti_6O_{13}$ were obtained with continuous stirring for 24 h. After they were washed with double-distilled water six times, the activated $K_2Ti_6O_{13}$ whiskers were dried in a vacuum-drying oven at 60°C until the quality was constant.

MPS (KH570) was used as the silane coupling agent for the surface vinyl modification of $K_2Ti_6O_{13}$. First, 0.5 g of MPS was dropped into a 32-mL mixture solution of ethanol/$H_2O$ (15:1 v/v). Subsequently, the pH of the mixed solution was adjusted by HAc to 1.5. The obtained solution mixture was stirred for 30 min. Then, 1 g of $K_2Ti_6O_{13}$, 100 mL of ethanol, and the solution mixture were added to a three-necked flask with continuous stirring. The modification continued for 4 h at 30°C. The product was centrifuged and washed repeatedly until the supernatant was neutral, and finally dried in the vacuum-drying oven at 60°C until the quality was constant.

### Preparation of the Quinoline–MIPs and Non-Imprinted Polymers (NIPs) Based on $K_2Ti_6O_{13}$

The quinoline–MIPs based on $K_2Ti_6O_{13}$ were prepared with a combination of SMIT and ATRP. First, quinoline (1 mmol) and MMA (3 mmol) were mixed in 50 mL of toluene, and the mixture solution was put in a refrigerator for 24 h to obtain the preassembly solution. Then, EGDMA (20 mmol) and vinyl-modified $K_2Ti_6O_{13}$ whiskers were added to another 50 mL of toluene, and the mixture was followed by sonication for 10 min. Both of the previous mixture solutions were further mixed in a flask with magnetic stirring; this was followed by the emission of $N_2$ and the exhaustion of $O_2$. Under the protection of $N_2$, CuBr (taken from vacuum drying oven), PMDETA and EBiB were added fleetly into the flask. The reaction proceeded at 60°C under the $N_2$ protection for 18 h. Finally, the process of centrifugation was repeated with the product, and it was washed six times and dried in the vacuum-drying oven. Non-imprinted polymers (NIPs) were prepared by the same procedure without the addition of quinoline. For MIPs, the elution of the templates was conducted with methanol/HAc (9:1 v/v) with Soxhlet extraction.

### Batch-Mode Binding Experiments

In the batch-mode binding experiments, *n*-octane was used as the solvent of simulated oil; this proved to be feasible in our previous studies.[27,29–31] Simulated oils with different concentrations of quinoline ranging from 10 to 100 mg/L were prepared. The concentrations of simulated oil were determined with gas chromatography (GC) with tetradecane as the internal standard.

The kinetic adsorption experiments were carried out at 298, 308, and 318 K, respectively. An amount of 10 mg of MIPs or NIPs was dispersed in 3 mL of simulated oil with a concentration of 50 mg/L. After it was shaken on a shaker at a frequency of 150 rpm for 10 time intervals from 5 min to 3 h, the adsorbed oil was centrifuged. The supernatant was sucked and filtered with a 0.22-$\mu$m organic filter membrane. The concentration was determined by GC with the temperature program of the column rising from 100 to 200°C at a heating rate of 15°C/min.

The isothermal adsorption experiments were conducted at 298, 308, and 318 K, respectively. An amount of 10 mg of MIPs or

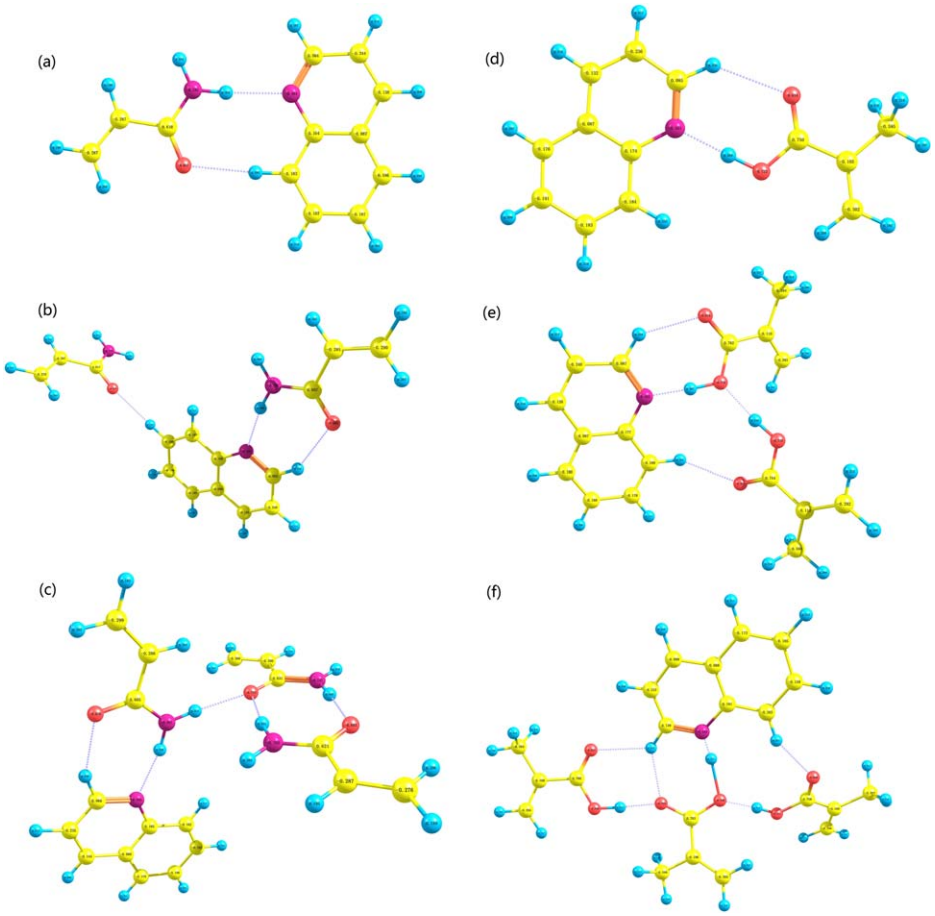


**Figure 3.** Minimum energy conformation, interaction mode, and NBO charge distribution of quinoline–monomer complexes with ratios of 1:1, 1:2, and 1:3. (In the online figure, the blue sphere represents hydrogen atoms, the yellow sphere represents carbon atoms, the red sphere represents oxygen atoms, and the purple sphere represents nitrogen atoms.) [Color figure can be viewed in the online issue, which is available at wileyonlinelibrary.com.]

NIPs was dispersed in 3 mL of simulated oil with different concentrations ranging from 10 to 100 mg/L. The adsorption time was set as 2 h to reach adsorption equilibrium. After filtration, the obtained supernatant was determined with the GC method.

The adsorption capacity at different times and the equilibrium adsorption capacity of quinoline were calculated with eqs. 2 and 3, respectively:

$$q_t = (C_0 - C_t)V/m \quad (2)$$

$$q_e = (C_0 - C_e)V/m \quad (3)$$

where $q_t$ and $q_e$ represent the adsorption capacity at time $t$ (mg/g) and the equilibrium adsorption capacity (mg/g), respectively; $C_0$, $C_t$, and $C_e$ are the concentrations of quinoline at the initial time, time $t$, and equilibrium, respectively (mg/L); $V$ (L) is the solution volume; and $m$ (g) is the mass of MIPs or NIPs.

### Selective Adsorption Experiments

Simulated oil containing a mixture of quinoline, indole, benzothiophene (BT), and dibenzothiophene (DBT) with a concentration of 50 mg/L for each substance was prepared. An amount of 10 mg of MIPs or NIPs was dispersed in 3 mL of simulated oil with four substances. After the solution was shaken on a shaker at 298 K (optimum temperature according to the batch-mode binding experiments) for 2 h, the supernatant was filtered and

**Table I.** Calculated $\Delta E$ Values of the Quinoline–Monomer Complexes

| Monomer | Ratio | $E_{quinoline}$ (au) | $E_{monomer}$ (au) | $E_{complex}$ (au) | $E_{BSSE}$ (au) | $\Delta E$ (au) | $\Delta E$ (kJ/mol) |
|---|---|---|---|---|---|---|---|
| AM | 1:1 | −401.9124 | −247.2919 | −649.2203 | 0.003497 | −0.01257 | −33.01 |
| | 1:2 | −401.9124 | −494.5837 | −896.5179 | 0.005002 | −0.01687 | −44.29 |
| | 1:3 | −401.9124 | −741.8756 | −1143.8471 | 0.010949 | −0.04821 | −126.58 |
| MAA | 1:1 | −401.9124 | −306.4711 | −708.4097 | 0.00464 | −0.02163 | −56.79 |
| | 1:2 | −401.9124 | −612.9421 | −1014.9006 | 0.010229 | −0.03601 | −94.54 |
| | 1:3 | −401.9124 | −919.4132 | −1321.4043 | 0.016713 | −0.06206 | −162.94 |

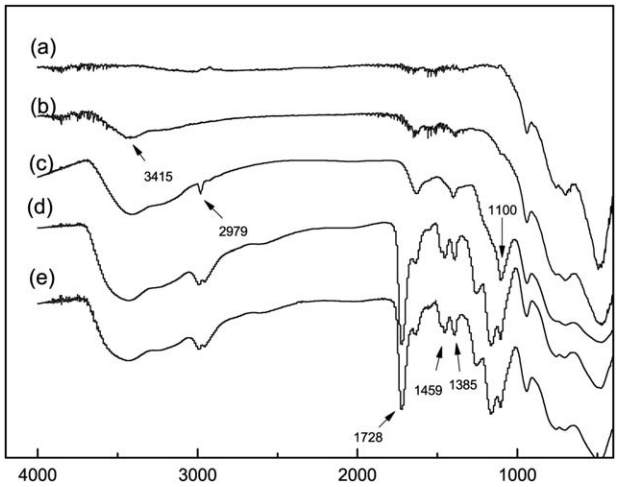


**Figure 4.** FTIR spectra of (a) $K_2Ti_6O_{13}$, (b) activated $K_2Ti_6O_{13}$, (c) MPS–$K_2Ti_6O_{13}$, (d) quinoline–MIPs, and (e) NIPs.

measured. The distribution coefficient ($K_d$; mL/g), selectivity coefficient ($K$), and relative selectivity coefficient ($K'$) of quinoline, indole, BT, and DBT were calculated with eqs. (4–6), respectively:

$$K_d = q_e/C_e \tag{4}$$

$$K = K_{\mathrm{d}}(quinoline)/K_{\mathrm{d}}(X) \tag{5}$$

$$K' = K_{\mathrm{MIP}}/K_{\mathrm{NIP}} \tag{6}$$

where $q_e$ is the adsorption equilibrium capacity of quinoline; $X$ represents indole, BT, or DBT; $K_{\mathrm{MIP}}$ is the selectivity coefficient of MIP; and $K_{\mathrm{NIP}}$ is the selectivity coefficient of NIP.

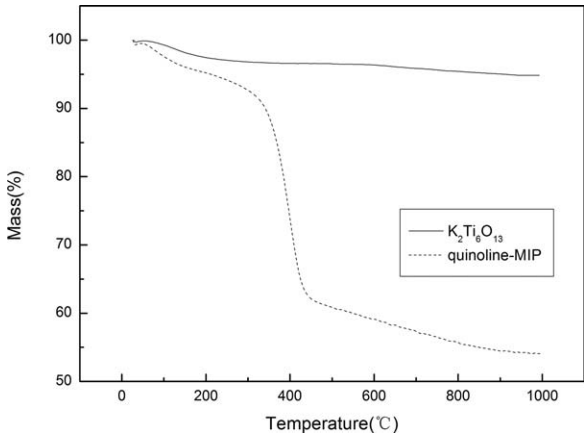


**Figure 6.** TGA curves of the $K_2Ti_6O_{13}$ and quinoline–MIPs.

## RESULTS AND DISCUSSION

### Molecular Simulation of the Imprinted Preassembly System

Two aspects, including the NBO charge transfer and $\Delta E$, were analyzed on the basis of the results of molecular simulation. Figure 2 presents the minimum energy conformation and NBO charge distribution of quinoline, AM, and MAA. Figure 3 presents the minimum energy conformation, interaction mode, and NBO charge distribution of quinoline–monomer complexes with ratios of 1:1, 1:2, and 1:3. The detailed data of the NBO charge distribution are listed in Table S1–S3 in the Supporting Information. When the ratio of quinoline to AM was 1:1, obvious charge transfers occurred (nitrogen atoms and hydrogen atoms in quinoline, respectively, transferred charges of 0.048 and −0.040 and hydrogen atoms and oxygen atoms in AM, respectively, transferred charges of −0.040 and 0.048); this illustrated that an interaction force (conjectured to be an

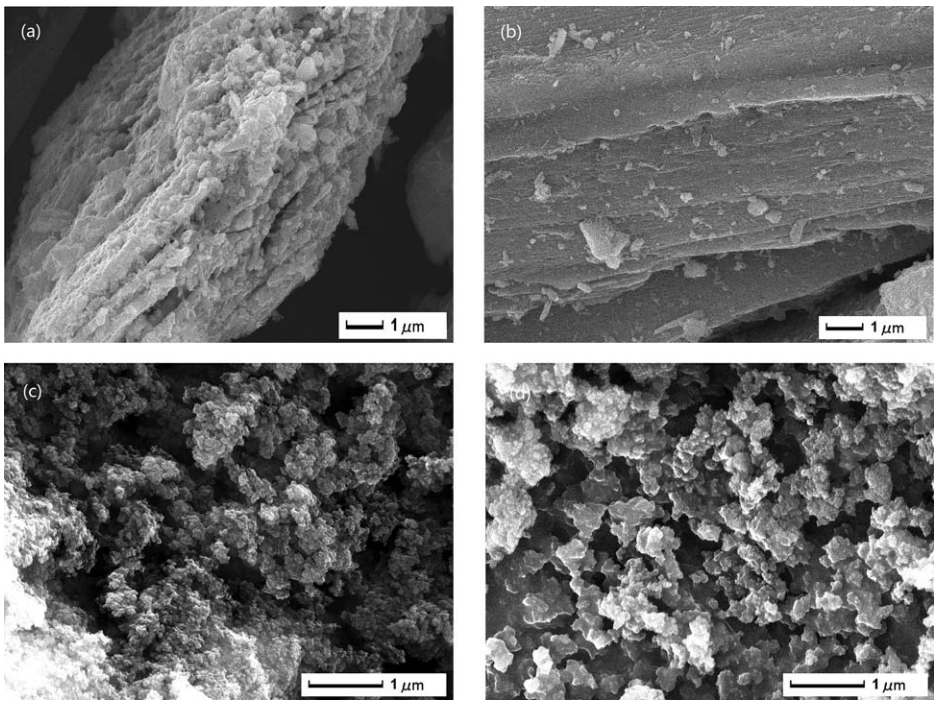


**Figure 5.** SEM images of the (a,b) $K_2Ti_6O_{13}$ whiskers, (c) quinoline–MIPs, and (d) NIPs.

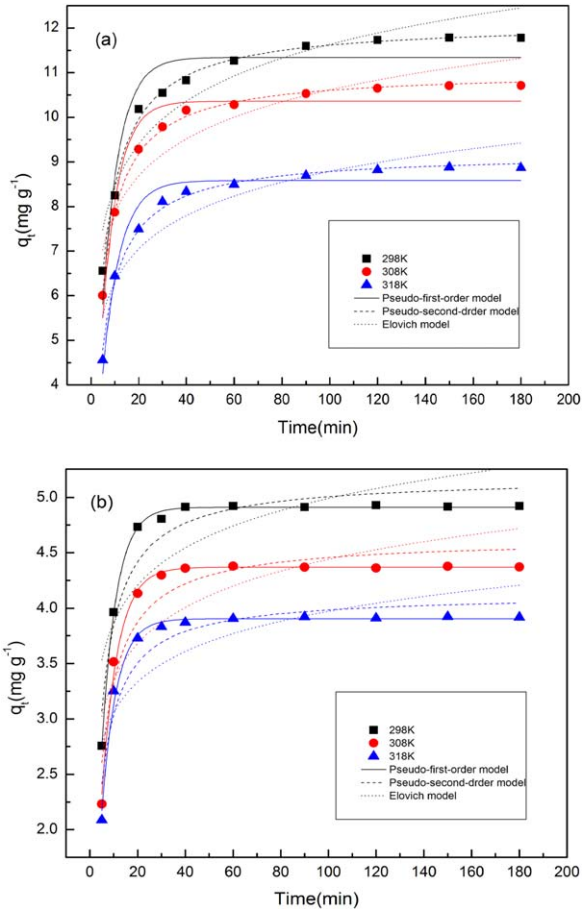


**Figure 7.** Adsorption kinetics of the (a) quinoline–MIPs and (b) NIPs at 298, 308, and 318 K. [Color figure can be viewed in the online issue, which is available at wileyonlinelibrary.com.]

N—H···N classical hydrogen bond and C—H···O nonclassical hydrogen bond[32–34]) formed between quinoline and AM. When the ratio between quinoline and AM was 1:2, except in the N—H···N bond and C—H···O bond forming between quinoline and the first AM, quinoline and the second AM also formed a C—H···O bond (the charge transfers of H and O were −0.038 and 0.027, respectively). As the ratio between quinoline and AM increased to 1:3, the situation became undesirable (only one AM monomer formed interactions with quinoline, and the three AM monomers formed interaction based on N—H···O bond); this illustrated that the amount of functional monomer did not mean the more, the better. When MAA was used as the functional monomer with a template–monomer ratio of 1:1, O—H···N and C—H···O bonds formed (the nitrogen atoms and hydrogen atoms in quinoline, respectively, transferred charges of 0.066 and −0.045, and hydrogen atoms and oxygen atoms in AM, respectively, transferred charges of −0.024 and 0.056). When the ratio between quinoline and MAA was 1:2, three hydrogen bonds, including one O—H···N bond and two C—H···O bonds, formed between quinoline and the MAA monomer. Compared with the use of AM with a ratio of 1:2, the distinction was that the two MAA monomers also formed a hydrogen-bond interaction. The interaction between the monomers strengthened the stability of the imprinted preassembly system on the premise of not weakening the interaction between the template and monomers. When the ratio between quinoline and MAA was 1:3, the favorable simulation result was exciting compared with the incapability of the same ratio between quinoline and AM.

Table I presents the $\Delta E$ values of the quinoline–monomer complexes after BSSE adjustment. As shown in Table I, we found that $E_{BSSE}$ could not be ignored compared with the uncorrected $\Delta E$. Therefore, the calculation of energy of BSSE ($E_{BSSE}$) was necessary. The corrected $\Delta E$ between quinoline and one AM monomer was 33.01 kJ/mol; this was attributed to an N—H···N classical hydrogen bond and a C—H···O nonclassical hydrogen bond. The corrected $\Delta E$ between quinoline and one MAA monomer resulting from an O—H···N bond and a C—H···O bond was 56.79 kJ/mol. This demonstrated that MAA could form stronger interaction forces with quinoline than with AM. As the template–monomer ratio increased to 1:2, $\Delta E$ between quinoline and MAA rose to 94.54 kJ/mol, whereas $\Delta E$ between quinoline and AM was only 44.29 kJ/mol. When the template–monomer ratio was 1:3, $\Delta E$ between quinoline and MAA was 162.94 kJ/mol, and $\Delta E$ between quinoline and AM also experienced a leap (126.58 kJ/mol). However, the leap of $\Delta E$ between quinoline and AM was attributed to hydrogen bonds forming between the AM monomers, and it was pointless.

By the combination of NBO charge-transfer analysis and $\Delta E$ analysis, the use of MAA as the functional monomer with a template–monomer ratio of 1:3 was found to be the optimum conditions for the quinoline-imprinted system. In the optimum quinoline-imprinted system, not only did the three MAA monomers form favorable hydrogen-bond interactions with quinoline, but also the hydrogen-bond interaction forming among the MAA monomers enhanced the stability of the imprinted system. Therefore, the preparation of the quinoline–MIPs and NIPs was conducted according to the simulation results.

### Characterization Methods

Figure 4 presents the FTIR spectra of $K_2Ti_6O_{13}$, activated $K_2Ti_6O_{13}$, MPS–$K_2Ti_6O_{13}$, quinoline–MIPs, and NIPs. After activation with HCl, the activated $K_2Ti_6O_{13}$ obtained hydroxyls on their surfaces {characteristic peak = 3415 cm$^{-1}$ in [Figure 9(b), shown later]}. Compared with the activated $K_2Ti_6O_{13}$ spectrum, the MPS–$K_2Ti_6O_{13}$ spectrum obviously showed new characteristic peaks, including —$CH_3$ stretching at 2979 cm$^{-1}$ and Si—O—Si asymmetric stretching at 1100 cm$^{-1}$. This demonstrated the successful grafting of MPS on $K_2Ti_6O_{13}$. After imprinting polymerization, the characteristic peaks at 1728 cm$^{-1}$ (C=O vibrations) and 1385 cm$^{-1}$ (C—H stretching) of EGDMA and the characteristic peak at 1459 cm$^{-1}$ (—COO— stretching) of MAA were obtained [Figure 9(d), shown later]. The spectrum of the NIPs [Figure 9(e), shown later] was similar to that of the quinoline–MIPs; this demonstrated that the templates in the prepared MIPs were almost completely removed.

Figure 5 presents the SEM images of the $K_2Ti_6O_{13}$ whiskers, quinoline–MIPs, and NIPs. As shown in Figure 5(a,b), the purchased $K_2Ti_6O_{13}$ whiskers possessed a compact and inerratic surface morphology. After the graft polymerization, the

**Table II.** Kinetic Parameters of the Quinoline–MIPs and NIPs Toward Quinoline

| | | Quinoline-MIPs | | | NIPs | | |
|---|---|---|---|---|---|---|---|
| Kinetic model | | 298 K | 308 K | 318 K | 298 K | 308 K | 318 K |
| | $q_{e,exp}$ (mg/g) | 11.781 | 10.711 | 8.872 | 4.922 | 4.373 | 3.918 |
| Pseudo-first-order | $q_{e,cal}$ (mg/g) | 11.343 | 10.361 | 8.584 | 4.912 | 4.371 | 3.906 |
| | $k_1$ ($min^{-1}$) | 0.144 | 0.154 | 0.137 | 0.164 | 0.151 | 0.163 |
| | $R^2$ | 0.9075 | 0.9344 | 0.9492 | 0.9986 | 0.9945 | 0.9909 |
| Pseudo-second-order | $q_{e,cal}$ (mg/g) | 12.123 | 11.031 | 9.19 | 5.178 | 4.63 | 4.13 |
| | $k_2$ (mg $g^{-1}$ $min^{-1}$) | 0.0189 | 0.0225 | 0.0236 | 0.0562 | 0.0556 | 0.0684 |
| | $R^2$ | 0.995 | 0.9971 | 0.9925 | 0.9195 | 0.9046 | 0.9019 |
| Elovich | $a$ (mg $g^{-1}$ $min^{-1}$) | 60.368 | 83.277 | 36.17 | 138.03 | 56.64 | 87.403 |
| | $b$ (g/mg) | 0.72 | 0.833 | 0.923 | 2.054 | 2.115 | 2.517 |
| | $R^2$ | 0.884 | 0.851 | 0.845 | 0.637 | 0.628 | 0.621 |

$q_{e,exp}$, adsorption capacity obtained by experiment; $q_{e,cal}$, adsorption capacity obtained by model fitting.

imprinted polymer layer was coated on the surface of the modified $K_2Ti_6O_{13}$ whiskers. In contrast, as shown in Figure 5(c,d), the MIPs possessed a rougher surface morphology and a greater number of pores than the NIPs; this was attributed to the addition of quinoline during the imprinted polymerization and the formation of imprinted recognition sites after the elution of the templates.

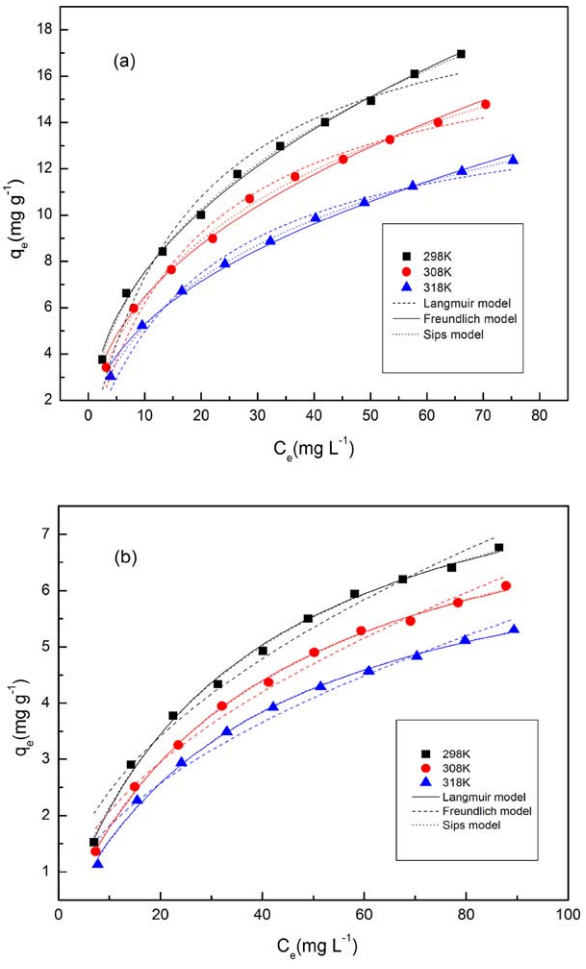


**Figure 8.** Adsorption isotherms of the (a) quinoline–MIPs and (b) NIPs at 298, 308, and 318 K. [Color figure can be viewed in the online issue, which is available at wileyonlinelibrary.com.]

Figure 6 presents the TGA curves of the $K_2Ti_6O_{13}$ and quinoline–MIPs. In the $K_2Ti_6O_{13}$ TGA curve, the mass loss within 100°C resulted from the adsorbed free water. After that, the curve leveled off; this demonstrated the favorable thermostability of the $K_2Ti_6O_{13}$ whiskers. For the quinoline–MIP TGA curve, a dramatic mass decline was observed from 318 to 447°C. This was attributed to the mass loss of the imprinted polymer layer. The grafting yield of the imprinted layer was about 31.35%. From 447 to 1000°C, the relatively low mass loss was attributed to the loss of the grafted MPS.

### Adsorption Kinetics Analysis

To confirm the adsorption equilibrium time exactly and determine the adsorption mechanism to some extent, batch-mode experiments of adsorption kinetics were conducted, and the experimental data were fitted and analyzed. In this study, three fitting models of adsorption kinetics, including a pseudo-first-order kinetics model, pseudo-second-order kinetics model, and Elovich model were used. They are given by eqs. (7–9), respectively:

$$q_t = q_e(1 - e^{-k_1 t}) \quad (7)$$

$$q_t = q_e^2 k_2 t/(1 + q_e k_2 t) \quad (8)$$

$$q_t = \ln(ab)/b + \ln t/b \quad (9)$$

where $t$ is the adsorption time; $k_1$ and $k_2$ represent the adsorption rate constants of the pseudo-first-order and pseudo-second-order, respectively; a represents the initial adsorption rate; and b is a constant related to the surface coverage.

Figure 7 and Table II present the fitting curves and fitting data of the adsorption kinetics of the prepared MIPs and NIPs. For all six adsorption kinetics curves of the MIPs and NIPs, in the initial adsorption stage, the adsorption rate was maintained at a high level. As time went on, the adsorption rate become lower and lower until the adsorption achieved equilibrium. The linear

**Table III.** Adsorption Isothermal Parameters of the Quinoline–MIPs and NIPs Toward Quinoline

| | | Quinoline–MIPs | | | NIPs | | |
|---|---|---|---|---|---|---|---|
| Isotherm models | | 298 K | 308 K | 318 K | 298 K | 308 K | 318 K |
| Langmuir | $k_L$ (L/mg) | 0.0554 | 0.052 | 0.0481 | 0.0294 | 0.026 | 0.026 |
| | $q_{mL}$ (mg/g) | 20.538 | 18.102 | 15.287 | 9.316 | 8.628 | 7.531 |
| | $R^2$ (nonlinear) | 0.9677 | 0.9805 | 0.9849 | 0.9967 | 0.9981 | 0.9974 |
| Freundlich | $K_F$ | 2.7946 | 2.4062 | 1.9634 | 0.7886 | 0.6439 | 0.5648 |
| | $n_F$ | 2.318 | 2.325 | 2.336 | 2.0449 | 1.9681 | 1.9751 |
| | $R^2$ (nonlinear) | 0.9972 | 0.9929 | 0.9941 | 0.9787 | 0.9823 | 0.976 |
| Sips | $q_{ms}$ (mg/g) | 81.093 | 33.143 | 26.231 | 9.7623 | 9.075 | 7.3074 |
| | $a_s$ | 0.01 | 0.0098 | 0.0111 | 0.0263 | 0.0233 | 0.0278 |
| | $n_s$ | 2.0018 | 1.6263 | 1.5735 | 1.0534 | 1.0512 | 0.9677 |
| | $R^2$ (nonlinear) | 0.9976 | 0.9969 | 0.999 | 0.9965 | 0.9981 | 0.9972 |

adsorption in the initial adsorption stage was mainly attributed to the surface diffusion, whereas the subsequent nonlinear adsorption was mainly attributed to intraparticle diffusion. It was obvious that the NIPs reached adsorption equilibrium much earlier than the MIPs. The difference was in the relatively long nonlinear adsorption process of the MIPs compared with the NIPs. Therefore, the adsorption process of the NIPs mainly relied on surface diffusion, whereas that of the MIPs involved both surface diffusion and intraparticle diffusion; this could be explained exactly by the successfully obtained imprinted sites of the MIPs. On the basis of the adsorption kinetics, 2 h was confirmed as the adsorption equilibrium time for the following experiments of adsorption isotherms and adsorption selectivity. In addition, the adsorption capacities of the MIPs and NIPs at 298 K was obviously higher than those at 308 or 318 K; therefore, 298 K was selected as the optimum adsorption temperature in our study.

As shown in Table II, the correlation coefficients ($R^2$'s) of pseudo-second-order kinetics fitting for the MIPs and pseudo-first-order kinetics fitting for the NIPs were above 0.99. All of the results demonstrate that the adsorption process of the prepared quinoline–MIPs fit pseudo-second-order kinetics well and that of the NIPs fit pseudo-first-order kinetics well. The errors between the experimental values and the calculated values (fitted kinetics model) were all less than 5%.

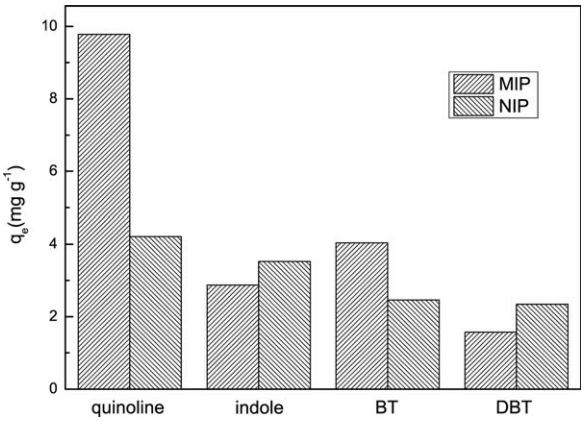


**Figure 9.** Adsorption selectivity of the quinoline–MIPs and NIPs toward quinoline and its analogues.

### Adsorption Isotherm Analysis

To depict and determine the adsorption properties of the prepared MIPs, the data of adsorption isotherm were fitted with three kinds of adsorption isotherms models, including the Langmuir, Freundlich, and Sips models. The Langmuir and Freundlich models, with two parameters, are common adsorption isotherm models for describing the adsorption process, and the Sips model, with three parameters, is generally used to describe nonuniform surface adsorption and transforms into the Langmuir or Freundlich models according to the adsorption conditions. The three adsorption isotherm models are given in eqs. (10–12), respectively:

$$q_e = q_{mL}k_LC_e/(1+k_LC_e) \quad (10)$$

$$q_e = k_F{C_e}^{1/n_F} \quad (11)$$

$$q_e = [q_{ms}(a_sC_e)^{1/n_s}]/[1+(a_sC_e)^{1/n_s}] \quad (12)$$

where $q_{mL}$ is the maximum adsorption capacity of monolayer adsorption (mg/g); kL is the Langmuir constant (L/mg); $K_F$ and $n_F$ are Freundlich constants representing adsorption capacity and intensity, respectively; $q_{ms}$ is a constant related to the adsorption capacity; $a_s$ is a constant related to the adsorption energy; and $n_s$ expresses the uniformity of adsorption.

Figure 8 and Table III present the fitting curves and fitting data, respectively, of the adsorption isotherm of the prepared MIPs and NIPs. As shown in Figure 8, three isotherm curves at different temperatures had the similar tendencies. As $C_e$ increased, the adsorption capacity increased. However, the growth rate of the adsorption capacity became lower and lower. Because of the restriction of the low concentration range of quinoline in our study, the isotherms curves did not reach equilibration. The temperature had an obvious effect on the adsorption capacities of the MIPs and NIPs. The adsorption capacities of the MIPs were ranked in descending order as follows: MIPs at $298 > 308 > 318$ K. Therefore, compared with 308 and 318 K, 298 K was the optimum temperature for the adsorption process

**Table IV.** Selective Binding Parameters of the Quinoline–MIPs and NIPs Toward Quinoline

| | Quinoline–MIPs | | | NIPs | | | |
|---|---|---|---|---|---|---|---|
| Mixed solution | $Q_e$(mg/g) | $K_d$ (L/g) | $K$ | $Q_e$(mg/g) | $K_d$ (L/g) | $K$ | $K'$ |
| Quinoline | 9.78 | 0.321 | — | 4.21 | 0.101 | — | |
| Indole | 2.87 | 0.0648 | 4.954 | 3.52 | 0.0819 | 1.233 | 4.02 |
| BT | 4.04 | 0.0964 | 3.33 | 2.46 | 0.0546 | 1.85 | 1.8 |
| DBT | 1.57 | 0.0335 | 9.582 | 2.34 | 0.0516 | 1.957 | 4.896 |

in this study. For the fitting results, we observed visually that the adsorption process of the MIPs all fit the Freundlich model better than the Langmuir model; however, that of the NIPs followed the opposite pattern.

As shown in Table III, the R2 values of the Freundlich and Sips model fitting of the MIPs were all above 0.99. For the NIPs, the isotherm models with a convinced degree of fitting ($R^2$ >0.99) were the Langmuir model and the Sips model. The difference of the fitting results could be explained by the difference in the adsorption mechanism. The adsorption process of the MIPs involved both surface diffusion and intraparticle diffusion; however, that of the NIPs mainly depended on surface diffusion. The value of 1/nF in the Freundlich equation has a positive correlation with the adsorption intensity. So, for the MIPs, the adsorption process at 298 K possessed the largest intensity. For the NIPs, in terms of the qmL values in the Langmuir equation, the adsorption process at 298 K had the largest qmL. According to previous studies,[35] the properties of NIPs reflect the properties of MIPs. In the Sips equation, the closer the value of $n_s$ is to 1, the more homogeneous the surface of the absorbent is. Therefore, both the MIPs and NIPs had a favorable uniformity of adsorption. The $n_s$ value of the NIPs was closer to that of the MIPs; this was attributed to the fact that the NIPs, without imprinted cavities, did not involve intraparticle diffusion.

### Adsorption Selectivity Analysis

Adsorption selectivity experiments were carried to determine whether the prepared MIPs were selective toward quinoline.

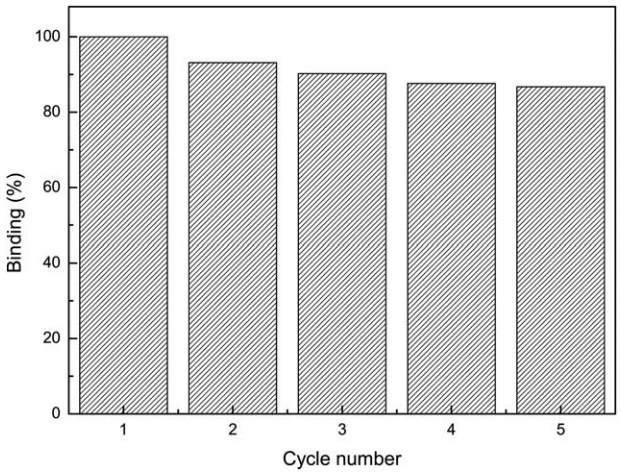


**Figure 10.** Reusability of the quinoline–MIPs after five cycles.

Three substances, including indole, BT, and DBT, were chosen as quinolone's structural analogues. Figure 9 visually presents the results of the adsorption selectivity. For the NIPs, the adsorption capacities toward the four substances had relatively little difference. However, for the MIPs, the adsorption capacity of quinoline had an evident superiority over those of the three analogues.

As shown in Table IV, with the functionality and advantages of imprinted sites, the quinoline–MIPs possessed more than two times the adsorption capacity of the NIPs, although the differences in the adsorption capacity toward quinolone's analogues between the MIPs and NIPs were far less than that toward quinoline. $K'$ could intuitively and accurately reflect the adsorption selectivity toward the analogues. The $K'$ value of the quinoline–MIPs toward indole and DBT were all above 4.0 (4.02 and 4.896, respectively). The high $K'$ value was attributed to the differences in the structure, functional groups, and spatial conformation of imprinted sites between quinoline and indole/DBT. Although the $K'$ of the quinoline–MIPs toward BT (1.8) were not as good as those of the previous two, it was acceptable according to previous studies. All of the previous results demonstrated the selectivity of the prepared quinoline–MIPs.

### Regeneration of the Quinoline–MIPs

It was necessary to investigate the regeneration ability of the quinoline–MIPs for their repeated cycle use. The quinoline–MIPs, which achieved adsorption equilibrium, were eluted with a mixed solution of methanol/acetic acid (9:1 v/v) until quinoline could not be determined in the eluant. The eluted quinoline–MIPs adsorbed quinoline at 298 K for 2 h repeatedly. The regeneration experiment was repeated five times. Figure 10 presents the results of the regeneration experiment. After five cycles of adsorption/desorption, the adsorption capacity of the quinoline–MIPs achieved a loss of 13.27% compared with the initial adsorption capacity; this indicated that the quinoline–MIPs prepared in this study possessed a favorable regeneration ability.

## CONCLUSIONS

Toward the common nitride quinoline in fuel oil, MIT was used to rationally prepare a novel adsorbent with favorable selectivity. The quinoline-imprinted preassembly systems with AM/MAA as a functional monomer, with ratios of 1:1, 1:2, and 1:3, were simulated by DFT. The simulation result revealed that MAA was more suitable as a functional monomer toward quinoline. The imprinted preassembly system with MAA as a monomer with a template–monomer ratio of 1:3 was the optimum system in this study. In the optimum imprinted system, not only all three

MAAs formed strong hydrogen-bond interactions with quinoline, but also the hydrogen-bond interactions formed among the MAA monomers increased the stability of system. As advanced preparation methods of MIPs, SMIT and ATRP were combined for the preparation of quinoline–MIPs on the basis of the previous simulation results. The adsorption kinetics of the quinoline–MIPs and NIPs toward quinoline were fitted with the pseudo-second-order kinetics model and pseudo-first-order kinetics model, respectively. The adsorption isotherms of the quinoline–MIPs and NIPs were fitted with the Freundlich and Langmuir models, respectively. The difference of the fitting results reflected the difference in the adsorption mechanisms between the quinoline–MIPs and NIPs. The selective adsorption ability of the quinoline–MIPs was demonstrated with indole, BT, and DBT as analogues through equilibrium binding analysis. In addition, the regeneration ability of the quinoline–MIPs was demonstrated to be favorable. This study will provide needful guidance and a theoretical basis for the preparation of imprinted materials in the field of industrial denitrification.

## ACKNOWLEDGMENTS

This work was supported by the National Basic Research Program of China (973 Program, contract grant number 2012CB821500), National Natural Science Fund (contract grant number 21106056 and 21174057), Jiangsu Natural Science Foundation of China (contract grant number BK2011512), and Senior Talent Foundation of Jiangsu University (contract grant number 14JDG057).

## REFERENCES

1. Oliveira, E. C.; De Campos, M. C. V.; Lopes, A. S.; Vale, M. G. R.; Caramao, E. B. J. *Chromatogr. A* **2004**, *1027*, 171.
2. Laredo, G. C.; Vega-Merino, P. M.; Rejio-Zarraga, F. T.; Castillo, J. *Fuel Process. Technol.* **2013**, *106*, 21.
3. Laredo, G. C.; Altamirano, E.; De los Reyes, J. A. *Appl. Catal. A* **2003**, *243*, 207.
4. Xiang, C. E.; Chai, Y. M.; Liu, Y. Q.; Liu, C. G. J. *Fuel. Chem. Technol.* **2008**, *29*, 595.
5. Gaudino, E. C.; Carnaroglio, D.; Boffa, L.; Cravotto, G.; Moreira, E. M.; Nunes, M. A. G.; Dressler, V. L.; Flores, E. M. M. *Ultrason. Sonochem.* **2014**, *21*, 283.
6. Cheng, H. B.; Kumar, M.; Lin, J. G. *Int. Biodeterior. Biodegrad.* **2012**, *67*, 28.
7. Ma, S. C.; Jin, Y. J.; Jin, X.; Yao, J. J.; Zhang, B.; Dong, S.; Dan, R. X. *J. Fuel Chem. Technol.* **2011**, *39*, 460.
8. Ahmed, I.; Hasan, Z.; Khan, N. A.; Hasan, Z.; Jhung, S. H. *J. Hazard. Mater.* **2013**, *250*, 37.
9. Zhang, H.; Li, G.; Jia, Y. H.; Liu, H. O. *J. Chem. Eng. Data* **2010**, *55*, 173.
10. Pichon, V.; Chapuis-Hugon, F. *Anal. Chim. Acta* **2008**, *622*, 48.
11. Kubo, T.; Hosoya, K.; Otsuka, K. *Anal. Sci.* **2014**, *30*, 97.
12. Shen, X. T.; Xu, C. G.; Ye, L. *Ind. Eng. Chem. Res.* **2012**, *52*, 13890.
13. Mafu, L. D.; Msagati, T. A. M.; Mamba, B. B. *Environ. Sci. Pollut. R.* **2013**, *20*, 790.
14. Hu, Y. L.; Wang, Y. Y.; Chen, X. G.; Hu, Y. F.; Li, G. K. *Talanta* **2010**, *80*, 2099.
15. Fernandez-Gonzalez, A.; Guardia, L.; Badia-Laino, R.; Diaz-Garcia, M. E. *Trac.-Trend. Anal. Chem.* **2006**, *25*, 949.
16. Gong, X. Y.; Cao, X. J. *J. Biotechnol.* **2011**, *153*, 8.
17. Xu, P. P.; Xu, W. Z.; Zhang, X. J.; Yan, Y. S. *Microchim. Acta* **2010**, *171*, 441.
18. Yang, Y. Z.; Liu, X. G.; Guo, M. C. *Colloid Surf. A* **2011**, *377*, 379.
19. Mamada, A.; Tanaka, T.; Kungwatchakun, D. *Macromolecules* **1990**, *23*, 1517.
20. Lee, M. H.; Thomas, J. L.; Ho, M. H.; Yuan, C.; Lin, H. Y. *ACS Appl. Mater. Int.* **2010**, *2*, 1729.
21. Xu, W. Z.; Zhou, W.; Huang, W. H.; Pan, J. M.; Li, H.; Wu, X. Y.; Yan, Y. S. *Microchim. Acta* **2011**, *175*, 167.
22. Wang, J. S.; Matyjaszewski, K. J. *Am. Chem. Soc.* **1995**, *117*, 5614.
23. Zhang, H. Q. *Eur. Polym. J.* **2013**, *49*, 579.
24. Pardeshi, S.; Dhodapkar, R.; Kumar, A. *Spectrochim. Acta A* **2013**, *116*, 562.
25. Nicholls, I. A.; Andersson, H. S.; Charlton, C.; Henschel, H.; Karlsson, B. C. G.; Karlsson, J. G.; O'Mahony, J.; Rosengren, A. M.; Rosengren, K. J.; Wikman, S. *Biosens. Bioelectron.* **2009**, *25*, 543.
26. Nicholls, I. A.; Karlsson, B. C. G.; Olsson, G. D.; Rosengren, A. M. *Ind. Eng. Chem. Res.* **2013**, *52*, 13900.
27. Yang, W. M.; Liu, L. K.; Zhou, Z. P.; Liu, H.; Xie, B. Z.; Xu, W. Z. *Appl. Surf. Sci.* **2013**, *282*, 809.
28. Balabin, R. M. *J. Chem. Phys.* **2008**, *129*, 164101.
29. Yang, W. M.; Liu, L. K.; Zhou, Z. P.; Qiu, C. X.; Ma, P. F.; Liu, H.; Xu, W. Z. *New J. Chem.* **2013**, *37*, 2758.
30. Cao, Y.; Liu, L. K.; Xu, W. Z.; Wu, X. Y.; Huang, W. H. *J. Appl. Polym. Sci.* **2014**, *131*, 40473.
31. Liu, L. K.; Cao, Y.; Ma, P. F.; Qiu, C. X.; Xu, W. Z.; Liu, H.; Huang, W. H. *RSC Adv.* **2014**, *4*, 605.
32. Gautam, R. D. *Acc. Chem. Res.* **1991**, *24*, 290.
33. Weiss, M. S.; Brandl, M.; Suhnel, J.; Pal, D.; Hilgenfeld, R. *Trends Biochem. Sci.* **2001**, *26*, 521.
34. Badu, M. M.; Singh, S. K.; Balaram, P. *J. Mol. Biol.* **2002**, *322*, 871.
35. Baggiani, C.; Giovannoli, C.; Anfossi, L.; Passini, C.; Baravalle, P.; Giraudi, G. *J. Am. Chem. Soc.* **2012**, *134*, 1513.